



HAL
open science

ASSIMILATION OF DISCHARGE DATA INTO SEMI-DISTRIBUTED CATCHMENT MODELS FOR SHORT TERM FLOW FORECASTING: CASE STUDY OF THE SEINE RIVER BASIN

Simon Munier, Xavier Litrico, Gilles Belaud, Charles Perrin

► **To cite this version:**

Simon Munier, Xavier Litrico, Gilles Belaud, Charles Perrin. ASSIMILATION OF DISCHARGE DATA INTO SEMI-DISTRIBUTED CATCHMENT MODELS FOR SHORT TERM FLOW FORECASTING: CASE STUDY OF THE SEINE RIVER BASIN. *Journal of Hydrologic Engineering*, 2014, 20, pp.05014021. 10.1061/(ASCE)HE.1943-5584.0001054 . hal-01162521

HAL Id: hal-01162521

<https://hal.science/hal-01162521>

Submitted on 11 Jun 2015

HAL is a multi-disciplinary open access archive for the deposit and dissemination of scientific research documents, whether they are published or not. The documents may come from teaching and research institutions in France or abroad, or from public or private research centers.

L'archive ouverte pluridisciplinaire **HAL**, est destinée au dépôt et à la diffusion de documents scientifiques de niveau recherche, publiés ou non, émanant des établissements d'enseignement et de recherche français ou étrangers, des laboratoires publics ou privés.

1 **ASSIMILATION OF DISCHARGE DATA INTO**
2 **SEMI-DISTRIBUTED CATCHMENT MODELS FOR SHORT**
3 **TERM FLOW FORECASTING: CASE STUDY OF THE SEINE**
4 **RIVER BASIN**

5 Simon Munier¹, Not a member, ASCE

 Xavier Litrico², Member, ASCE

 Gilles Belaud³, Not a member, ASCE

 and Charles Perrin⁴, Not a member, ASCE

6 **ABSTRACT**

7 This study addresses the sensitivity of short-term flow forecasting in the Seine River basin
8 (43,800 km², France) to the spatial distribution using a semi-distributed model (*Transfer*
9 *with GR*, TGR). The basin was decomposed into intermediate basins depending on the
10 gauging stations selected for this study. A lumped hydrological model was applied on each
11 intermediate basin and a routing model was used to propagate the discharge through the
12 river network. Discharge data at the gauging stations were assimilated using a Kalman filter
13 and tests for flow forecasting were performed with a lead time up to 72 h. Several spatial
14 configurations, defined by a selection of one or several gauging stations, were tested and
15 the performances were compared to a reference lumped model currently used operationally
16 by the regional flood forecasting centre. Results showed that the forecasting performance
17 improves with an increase in the degree of spatialization. Nevertheless this improvement was
18 not systematic and the integration of some particular gauging stations degraded the model

¹Estellus, 93 boulevard de Sébastopol, 75002 Paris, France. simon.munier@gmail.com.

²LyRE, R&D center of Lyonnaise des Eaux, 91 rue Paulin, 33029 Bordeaux, France. xavier.litrico@lyonnaise-des-eaux.fr.

³Montpellier SupAgro, UMR G-EAU, 2 place Pierre Viala, 34060 Montpellier Cedex 1, France. belaud@supagro.inra.fr.

⁴Irstea, UR HBAN, 1 rue Pierre-Gilles de Gennes, CS 10030, 92761 Antony Cedex, France. charles.perrin@irstea.fr.

19 performance. In addition, it was shown that integrating some other stations (generally
20 the most upstream) led to a negligible improvement. This suggests that in an operational
21 context, where the model has to be robust and computationally efficient, some efforts should
22 focus on finding the optimal spatial distribution, which is not necessarily the one using all
23 the available stations.

24 **Keywords:** flow forecasting, spatial distribution, semi-distributed model, hydrology, routing
25 model, lumped model, Seine River

26 INTRODUCTION

27 Flood forecasting remains a difficult issue for hydrologists (see e.g., Young 2002; Todini
28 2007; Liu et al. 2012). In spite of a variety of available models and tools (see Cloke and
29 Pappenberger 2009, and references therein), the improvements in flood forecasting tools are
30 slow and there is large margin of progress (Kealey 2007; Welles et al. 2007). Namely, the
31 role of spatial distribution on model efficiency remains a matter of debate in the hydrological
32 community. In a flood forecasting context, the sensitivity of model forecasts quality seems
33 dependent on various physical factors and sources of uncertainty. The lumped approach,
34 though simple, find limitations for events showing a large spatial variability (see e.g., Cole
35 and Moore 2009). Similarly, fully distributed models do not appear to be the panacea
36 given their complexity and their lack of overall superiority (Smith et al. 2012). Hence semi-
37 distributed approaches are often considered as a good trade-off between complexity and
38 efficiency (see e.g., Amengual et al. 2008). Indeed, they couple rainfall-runoff models on
39 sub-catchments (here defined by gauging stations) and simple propagation tools like unit
40 hydrographs or lag-and-route methods (see e.g., Lerat et al. 2012). In a forecasting context,
41 one key issue is to simultaneously assimilate the information available in real-time. This may
42 be spatially distributed data like snow cover in mountainous regions (see e.g., Nester et al.
43 2012) or more classically the flow observations at the gauging stations within the catchment
44 (Mendoza et al. 2012).

45 This study focuses on a large catchment in France, the Seine River upper basin at Paris

46 (43,800 km²), where there are major socio-economic potential impacts in the capital city
47 of Paris. The regional flood forecasting centre (FFC) based in Paris is in charge of rou-
48 tinely issuing forecasts on the Seine and its tributaries to feed the national flood warning
49 map (www.vigicrues.gouv.fr). In flood conditions, the exceedance of warning thresholds is
50 forecasted to provide information for civilian security services, which ask for three-day an-
51 ticipation at Paris to have sufficient time for evacuating people and installing protections
52 against flooding (Lacaze et al. 2011). The FFC has implemented a forecasting system which
53 uses several hydrological and hydraulic models that are fed by hydro-meteorological obser-
54 vations and forecasts received in real-time. Among these models is a conceptual lumped
55 hydrological model which only simulates the discharge at the basin outlet, at which it was
56 calibrated. Due to its lumped structure (i.e. no explicit channel routing is made), it is not
57 able to simulate the discharge at upstream gauging stations and to account for informa-
58 tion available at these sites. However, it is likely that the information from these upstream
59 stations spread over the basin can be useful to improve forecasts at the basin outlet.

60 The objective of the study was to investigate the sensitivity of flood forecasts to the
61 spatial distribution of inputs and outputs using a semi-distributed hydrological model and
62 a Kalman-type real-time assimilation scheme. The Seine River basin was first decomposed
63 into several intermediate basins based on the location of the gauging stations. Then several
64 levels of spatial discretization were considered and the sensitivity of model performance at
65 the basin outlet with increasing spatial resolution was analysed. The semi-distributed model
66 has two main components: a hydrological module based on the lumped model and applied
67 on each intermediate basin, and a flow routing module representing the flow propagation be-
68 tween gauging stations. In order to check whether the semi-distributed model could provide
69 improvement over the lumped model, which is currently used in an operational context by
70 the French FFC, the performance of the semi-distributed model was benchmarked against
71 the performance of the lumped model used as a reference.

72 The next sections successively present the Seine River basin and the data used, the

73 forecasting model and the assimilation framework, and the testing methodology. Then results
74 are presented and discussed in section 5.

75 **THE SEINE RIVER UPPER BASIN AND AVAILABLE DATA**

76 The Seine River basin drains an area of 43,800 km² upstream of Paris, which is the outlet
77 considered in this study. From upstream to downstream, three major tributaries contribute
78 to the flow of the Seine River: the Yonne, Loing and Marne Rivers. The rivers mainly
79 flow westwards. The relief is quite low over the basin with altitudes mainly below 500 m
80 except in the upper Yonne basin with altitudes up to 900 m, which makes this tributary the
81 most reactive within the basin (see e.g., Billen et al. 2009; Viennot et al. 2009 for a detailed
82 description of the basin).

83 Four large dams, with a total storage capacity of about 800 hm³ were built in the upper
84 part of the basin, on the Marne, Seine, Aube and Yonne Rivers, respectively. They are man-
85 aged to regulate downstream flows, especially for the Paris region, with the two objectives of
86 low-flow augmentation (for domestic, industrial and agricultural water supply) and flood al-
87 leviation (Villion 1997). Flooding is a major natural risk in the Paris region, as shown by the
88 consequences of the major 1910 flood. This flood reached 2,400 m³/s, which corresponds to
89 about a 100-year return period. It is estimated that such a flood would today directly impact
90 850,000 people who live in zones liable to flooding within the Paris region and cause direct
91 damages estimated to more than 10 billion Euros (<http://vertigo.revues.org/14339#ftn1>).
92 Hence the early anticipation of such events may help mitigating their catastrophic conse-
93 quences.

94 The basin is under an oceanic climate, with mean precipitations of 790 mm/yr, mean
95 temperature of 11.1°C, and mean potential evapotranspiration (PE) of 690 mm using the
96 Penman formula (average over the 1958-2011 period using the SAFRAN reanalysis, see
97 Vidal et al. 2010). Precipitation is almost evenly distributed within the year. A network
98 of 68 rain gauges were used in this study (see Fig. 1), as well as a network of 10 flow
99 gauging stations distributed over the basin (see details in Table 1). These ten stations

100 are part of the stations considered by the FFC in their operational forecasting system.
101 Four gauging stations (La Ferté-sous-Jouarre, Bazoches-lès-Bray, Courlon-sur-Yonne and
102 Episy) control a large part of the basin upstream Paris, with a cumulated area of 33,520
103 km² (i.e. 77% of the basin). They are all situated downstream of the dams and therefore
104 integrate the impact of dam management. Hence they are interesting to consider in a flood
105 forecasting context. Within the Yonne basin, four additional stations (Dornecy, Arcy-sur-
106 Cure, Dissangis and Aisy-sur-Armanon) were considered to better account for the upstream
107 part, which receives the largest cumulated rainfall amounts on the basin. An additional
108 upstream station (Châlon-sur-Marne) was also considered on the Marne River, given the
109 elongated shape of this catchment.

110 Hourly time series of rainfall, streamflow and PE were available over the 1991-2009 period.
111 Since there are many missing data before 1995, the 1991-1994 period will be used only as a
112 warm-up period. The percentage of missing values for the 1995-2009 is reasonable (see Table
113 1 for the gauging stations), except for the Bazoches-lès-Bray station for which no data were
114 available before 1999. Large flood events occurred in Paris in the years 1995, 1999, 2000
115 and 2001. The selected periods are therefore interesting for analysing the behaviour of the
116 model in high flow conditions.

117 **SEMI-DISTRIBUTED HYDROLOGY-ROUTING COUPLED MODEL**

118 This section details the semi-distributed model built in this study to investigate the
119 impact of spatial discretization. We first detail the way the basin was spatially split. Then the
120 structures of the hydrological and flow routing sub-models are described, before presenting
121 the assimilation framework used to run the coupled model in forecasting mode.

122 **The semi-distributed modelling approach**

123 *Modelling principle*

124 The coupled model simulates the discharge at each gauging station. Therefore it can
125 assimilate discharge observations at these stations and propagate the improvements due
126 to state corrections downstream. The semi-distributed approach adopted in this study is

127 intermediate between lumped and fully distributed approaches. It divides the basin into
128 hydraulically connected sub-catchments.

129 Here, we aim at representing the discharge at the gauging stations on the main streams.
130 However we do not need to know the exact states of the system between these target points.
131 Therefore the intermediate basins were defined between these stations. Here an intermediate
132 basin is defined by an outlet (corresponding to a gauging station) and at least one (or possibly
133 several) upstream catchment (also defined by gauging stations). Therefore the intermediate
134 basin is the area that drains water to the river reach(es) between the downstream and the
135 upstream station(s).

136 For each intermediate basin, the model represents two types of water transfers (see Fig-
137 ure 2): the hydrological transfer represents the transformation of rainfall over the basin into
138 discharge that is injected into the main stream as lateral inflows, and the hydraulic transfer
139 (flow routing) corresponds to the discharge propagation through the main streams to a down-
140 stream station (see also Lerat et al. 2012). On upstream sub-basins, only the hydrological
141 part of the model is applied.

142 *Spatial discretization*

143 Regarding flow propagation in the main streams, the contribution to streamflow due to
144 rainfall on the intermediate basin may be considered as lateral inflows. The distribution of
145 this lateral discharge along the river stretch has an impact on the downstream discharge
146 (Fan and Li 2006; Munier 2009; Lerat et al. 2012). In the following, lateral flows will be
147 decomposed into concentrated or uniformly distributed lateral discharges. As shown in Fig-
148 ure 2, the flow routing module simulates the propagation of upstream and lateral discharges,
149 whereas the hydrological module simulates the total discharge due to rainfall. The output
150 of the hydrological module is injected into the routing module as lateral discharges following
151 an established longitudinal distribution depending on the hydrographic configuration of the
152 intermediate basin. As done by Lerat et al. (2012), we used the drained area curve to deter-
153 mine the spatial distribution of hydrological inputs. This curve is obtained from a Digital

154 Elevation Model and represents the area drained by the river stretch with respect to the
155 longitudinal abscissa (see Figure 2). It allows to locate the main tributaries which are con-
156 sidered as concentrated lateral inflows. The remaining surface is considered as a uniformly
157 distributed lateral inflow. The output of the hydrological model is then decomposed into
158 one or several lateral inflows (concentrated and distributed) weighted by their respective
159 draining areas. Munier (2009) showed that considering tributaries draining an area less than
160 20 % of the total intermediate basin area as concentrated lateral inflows does not improve
161 the simulation. The contribution of these tributaries are considered as distributed lateral
162 inflows. This criterion is used to limit the number of concentrated lateral inflows.

163 *Networking*

164 Considering the structure of the model, and especially the routing model, it is very simple
165 to couple multiple models representing multiple intermediate basins. For each intermediate
166 basin, the hydrological module computes the contribution due to rainfall, using rainfall and
167 evapotranspiration data over the intermediate basin. Then the routing module propagates
168 this lateral discharge as well as any observed upstream discharges (discharge at the outlet
169 of upstream basins) to compute the downstream discharge. Figure 3 shows an example
170 configuration: the discharge at station #5 results from the propagation of the discharge
171 at the four upstream stations (#1 to 4) and the flow produced in the intermediate basin
172 (between station #5 and stations #1 to 4); the discharge at the downstream station #6
173 results from the propagation of the flow at the upstream station #5 and the flow produced
174 on the intermediate basin (between stations #6 and 5).

175 **Model description**

176 *Hydrological model*

177 We used a lumped approach representing the rainfall-runoff transformation at the sub-
178 catchment (or intermediate catchment) scale. The hydrological model is derived from the
179 GR (*Génie Rural*) model developed by Berthet et al. (2009). It is defined by a production
180 store, a function representing surface-subsurface exchanges and a routing store. The GRP

181 model, an extension of the GR model, integrates a data assimilation procedure that allows
182 to correct the model states by assimilating the discharge at the outlet (Berthet et al. 2009).
183 The GRP (*Génie Rural-Prévision*) model is currently used in operational conditions by the
184 FFC for real-time forecasting.

185 In this study, the original GR model was coupled with a hydraulic linear model. The rout-
186 ing reservoir was linearized. Hence a linear Kalman filter is applied to correct the hydraulic
187 model states as well as the routing reservoir states. The linearised reservoir corresponds to
188 a first order filter like those defined in the flow routing model (see next section). Figure 4
189 presents the structure of the hydrological model. Three parameters must be calibrated for
190 each intermediate or upstream catchment:

- 191 • S (mm): the capacity of the production reservoir,
- 192 • IGF (-): the intercatchment groundwater function coefficient,
- 193 • K_R (s): the time constant of the routing reservoir.

194 Inputs of the hydrological model are the spatial average of precipitation P and potential
195 evapotranspiration PE over the intermediate basin. For each intermediate basin, PE is
196 computed from temperature and incoming radiation as done by Oudin et al. (2005) whereas
197 P is obtained from raingauges inside the basin.

198 *Flow routing model*

199 The flow routing model represents the discharge propagation through the river stretch.
200 It accounts for upstream and lateral (concentrated and uniformly distributed) discharges.
201 Many propagation models have been proposed in the literature, such as unit hydrographs or
202 Muskingum type models (e.g., Perumal et al. 2009). Nevertheless, such models are generally
203 not adapted to multiple inflows (unless by adding new parameters) and to data assimilation.
204 The model presented here is the propagation model developed by Munier (2009), hereafter
205 called LLR (standing for Linear Lag-and-Route). It has been chosen for its ability to account
206 for upstream as well as lateral inflows using a small number of parameters. Additionally, it

207 is particularly well adapted to data assimilation such as the Kalman filter.

208 The flow routing model is based on the Saint-Venant equations that describe the 1D free
209 surface flow dynamics. These equations, classically used to represent the flow propagation
210 in a river stretch, may be solved analytically after some simplifications. The main interest
211 of using these equations is that they are described by the physical characteristics of the
212 river stretch (geometry, roughness). Here, we used this property to describe the propagation
213 of every input discharges (upstream and lateral) using only two parameters, which limits
214 identifiability problems that may occur with over-parametrised models (see, e.g., Duan et al.
215 1992).

216 The Saint-Venant equations are first linearised around a uniform flow and transposed
217 into the frequential domain using the Laplace transform. Under this form, it is possible to
218 solve the equations analytically, leading to a linear transfer function between the upstream
219 and downstream discharges (Munier et al. 2008). Under the assumption of negligible upward
220 waves, transfer functions relating concentrated and uniformly distributed lateral flows to the
221 downstream discharge can be derived.

222 The river stretch is schematised as in Figure 5. In this section, the following notations
223 are used: t is the time (s), x the abscissa along the river stretch (m), X the length of the
224 river stretch (m), x_{Pi} the abscissa of the i -th concentrated lateral discharge (m), Q_0 the
225 upstream discharge (m^3/s), Q_X the downstream discharge (m^3/s), Q_{Pi} the i -th concentrated
226 lateral discharge (m^3/s), Q_D the uniformly distributed lateral discharge (m^3/s).

227 The derivation of transfer functions from the linearised Saint-Venant equations trans-
228 posed into the Laplace domain is given in Appendix S1 and leads to:

$$229 \quad Q_X(s) = TF_0(s)Q_0(s) + \sum_i TF_P(x_{Pi}, s)Q_{Pi}(s) + TF_D(s)Q_D(s) \quad (1)$$

230 where s denotes the Laplace variable, TF_0 , TF_P and TF_D the transfer functions related to
231 the upstream discharge and the concentrated and uniformly distributed lateral discharges,

232 respectively.

233 To compute the downstream discharge Q_X , Equation 1 has to be transposed back into
234 the time domain. In order to avoid high computation costs due to convolution algorithm,
235 the previous transfer functions are approximated by first order with delay transfer functions
236 using the Moment Matching Method, as done for example by Munier et al. (2008). Such
237 transfer functions have three main advantages: (1) they simulate the delay and attenuation
238 phenomena which characterise flow propagation, (2) they are easily transposed into the time
239 domain since they represent simple Ordinary Differential Equations (ODE) and (3) they are
240 particularly well suited to simple data assimilation techniques due to their linearity. The
241 three approximate transfer functions can then be written as:

$$242 \quad TF_0(s) \approx \frac{e^{-\tau_0 s}}{1 + K_0 s} \quad (2)$$

$$243 \quad TF_P(x_{Pi}, s) \approx \frac{e^{-\tau_P(x_{Pi})s}}{1 + K_P(x_{Pi})s} \quad (3)$$

$$244 \quad TF_D(s) \approx \frac{1}{1 + K_D s} \quad (4)$$

245 where τ_0 and τ_P are the delay values, K_0 , K_P and K_D the first order time constants. One
246 may note that TF_D has no delay, which can be explained by the fact that the distributed
247 lateral inflow is injected all along the river reach, and then right upstream the downstream
248 end.

249 Using analytical transformations (Laplace transform and Moment Matching Method),
250 the parameters of the approximate transfer functions can be expressed as functions of the
251 physical characteristics of the river stretch (see Appendix S2). These expressions can be
252 simplified in order to reduce the number of parameters. Indeed, $\tau_P(x_{Pi})$, $K_P(x_{Pi})$ and K_D

253 can be expressed as functions of x_{Pi}/X , τ_0 and K_0 .

$$254 \quad \begin{cases} \tau_P(x_{Pi}) = \left(1 - \frac{x_{Pi}}{X}\right) (\tau_0 + K_0) - \sqrt{1 - \frac{x_{Pi}}{X}} K_0 \\ K_P(x_{Pi}) = \sqrt{1 - \frac{x_{Pi}}{X}} K_0 \\ K_D = \frac{\tau_0 + K_0}{2} \end{cases} \quad (5)$$

255 Note that the delay parameter τ_P may reach negative values. Since such a case is physi-
256 cally unrealistic, the lower bound for τ_P was set to 0 and parameter K_P is computed conse-
257 quently:

$$258 \quad \text{If } \tau_P(x_{Pi}) < 0, \text{ then } \tau_P(x_{Pi}) = 0 \text{ and } K_P(x_{Pi}) = \left(1 - \frac{x_{Pi}}{X}\right) K_0 \quad (6)$$

259 Last, the flow routing model is described by three types of transfer functions related
260 to upstream, concentrated and uniformly distributed lateral discharges (Equations (2-4)).
261 The discretized form of such transfer functions is described in Appendix S3. If the relative
262 positions of the concentrated lateral discharges are known (x_{pi}/X), only two parameter
263 are necessary to define the model: the time delay τ_0 and the first order time constant K_0
264 related to the transfer of the upstream discharge. As stated earlier, these parameters can
265 be computed analytically from the physical characteristics of the river reach. Nevertheless,
266 simulation results may be improved if they are calibrated, which is done in this study.

267 *The TGR coupled model*

268 For an intermediate basin, the integrated model, named TGR for Transfer with GR (the
269 selected hydrological model), is obtained by coupling the two sub-models (flow routing and
270 hydrology). The flow routing part and the routing reservoir of the hydrology part are linear.
271 This linear part of TGR is named LRK. The remaining part of the hydrological model
272 (production reservoir and exchange function) is named GRK. Figure 6 presents the scheme
273 of the TGR model for an intermediate basin. For each intermediate basin, five parameters
274 must be identified (τ_0 , K_0 , K_R , S and IGF) using P , PE and Q_0 as inputs and Q_X as
275 output. The relative positions x_{Pi}/X are determined from the drained area curve. For

276 an intermediate basin with several upstream basins, the relative position of each upstream
277 discharge is also known, and the transfer of the upstream discharges is done consequently, as
278 for concentrated lateral inflows. For a sub-catchment basin with no upstream station, only
279 the hydrological model is applied and thus only the parameters related to the transformation
280 of rainfall into downstream discharge are identified. Several networks of possibly multiple
281 intermediate basins are presented in section 5 through the example of the Seine River upper
282 basin.

283 **Data assimilation for flood forecasting**

284 As pointed out by Liu et al. (2012), the manual correction of the model states by hu-
285 man forecasters, based on their expert interpretation of the discrepancies between model
286 simulations and observed discharges, is still widely practiced in operational forecasting. In
287 an operational context, data assimilation techniques allow to use observations received in
288 real-time to automatically correct the model outputs and refine the forecasts at each time-
289 step. Various assimilation techniques proposed in the literature can be applied for hydro-
290 logical forecasting (see e.g., Refsgaard 1997). Here we chose the widely used Kalman filter
291 (Kalman 1960). Indeed the coupled model presented in the previous section is particularly
292 well adapted to the Kalman filter, because of its linear part and the simplicity of the state
293 equations. The Kalman filter, which is applied on the linear part (LRK) of the TGR model,
294 is briefly described in the following.

295 Note that another Kalman filter, such as the Ensemble Kalman Filter (EnKF), could
296 have been used in order to correct not only the state variables of LRK, but also the state
297 variables of the non-linear part (GRK). Examples of existing ensemble flood forecasting
298 systems can be found in Cloke and Pappenberger (2009) and in McMillan et al. (2013).
299 However, as pointed out by Cloke and Pappenberger (2009) and Rabuffetti and Barbero
300 (2005), the characterization of meteorological input uncertainties, which have an important
301 impact in ensemble data assimilation procedures, remain a key challenge. In this paper,
302 the effect of including one or several upstream stations is investigated; the main physical

303 process involved is thus the flow routing between stations. As stated by Young (1974), most
304 of the non linearities come from the hydrological processes, the routing processes being more
305 linear, all the more so as only high flows are considered in the flood forecasting context.
306 Considering the robustness of the linear Kalman filter, it has been preferred here to more
307 sophisticated extensions.

308 The Kalman filter is applied to a discretized Linear Time-Invariant (LTI) model described
309 by the following equations:

$$310 \quad x(k) = A x(k-1) + B u(k) + w(k) \quad (7)$$

$$311 \quad y(k) = C x(k) + D u(k) + v(k) \quad (8)$$

312 where k is the discretized time, x the state of the system, u the input and y the output.
313 The input vector gathers the outputs of the GRK model applied on every upstream and
314 intermediate basins. The output vector represents the simulated discharges at every gauging
315 stations. In the LRK model, the output only depends on the state, so that the matrix D
316 is null. The random variables w and v represent the process noise and measurement noise,
317 respectively. They are supposed to be independent and described by a normal probability
318 law with covariance matrices Q for w and R for v . Both matrices are then diagonal. In
319 practice, process and measurement noise covariances are hardly quantifiable and are chosen
320 empirically. In this study the measurement noise is supposed to be lower than the process
321 noise, and values of R are consequently lower than those of Q . Besides, different tests
322 have been conducted to estimate the sensitivity of the forecast performances against values
323 of Q (presented in Munier 2009). Results showed that although the hydrological states
324 (those relative to the routing reservoir) are the most uncertain, little impact on the forecast
325 performances has been observed. Here, we chose a value of 1 for the process noise and 0.1
326 for the measurement noise.

327 The Kalman filter is described by the following equations:

$$328 \quad \hat{x}(k|k-1) = A \hat{x}(k-1|k-1) + B u(k) \quad (9)$$

$$329 \quad \tilde{y}(k) = y(k) - C \hat{x}(k|k-1) \quad (10)$$

$$330 \quad \hat{x}(k|k) = \hat{x}(k|k-1) + K(k) \tilde{y}(k) \quad (11)$$

331 where $\hat{x}(k|k-1)$ and $\hat{x}(k|k)$ are the prediction and the update states at time k , respectively,
332 y the measurements, $\tilde{y}(k)$ the measurement error (or innovation) and $K(k)$ a matrix called
333 the *Kalman Gain*. The corrected output is then given by:

$$334 \quad \hat{y}(k) = C \hat{x}(k|k) \quad (12)$$

335 Missing values are replaced by model prediction output given by $C\hat{x}(k|k-1)$. For in-
336 stance, if the i -th line of vector y is missing, then this line is replaced by the i -th line of the
337 model prediction output vector. This is equivalent to considering that the model is perfect
338 at this station.

339 The Kalman gain is computed so as to minimise the covariance $P(k|k)$ of the state error
340 $e(k|k) = x(k) - \hat{x}(k|k)$. The optimal Kalman gain is obtained from (e.g., Brown and Hwang
341 1992):

$$342 \quad K(k) = P(k|k-1)C^T (CP(k|k-1)C^T + R)^{-1} \quad (13)$$

343 where $P(k|k-1) = E[e(k|k-1)e(k|k-1)^T]$ is the covariance matrix of the prediction error
344 $e(k|k-1) = x(k) - \hat{x}(k|k-1)$.

345 Note that the LRK model, on which the Kalman filter is applied, represents the ensemble
346 of intermediate basins for a specific configuration. The Kalman Filter algorithm will then
347 assimilate the discharge at every considered gauging stations and simultaneously correct all
348 the states of the system.

349 TESTING METHODOLOGY

Split sample testing

The model was tested using the split-sample test proposed by Klemes (1986). It consists in splitting the available time series into two sub-periods (here, P1: 1994-2001 and P2: 2001-2009, including a 1-year warm-up period). The identification procedure is performed on P1 and the validation on P2, and then the role of the two periods is reversed (calibration on P2 and validation on P1). Thus the model can be evaluated in validation mode on the whole time span.

Parameter identification was done using the Levenberg-Marquardt algorithm with the root mean square errors (RMSE) criterion on the discharge at the outlet. For the application on the Seine River basin, the identification is done for each tested configuration and for each intermediate or upstream basin independently, i.e. using observed upstream flow data in the case of an intermediate basin. This procedure has two main advantages: it prevents the propagation of modelling errors from the upstream to the downstream basins and it reduces the amount of parameters to be identified simultaneously. Model parameters were calibrated in simulation mode, i.e. without considering the assimilation scheme.

In validation, the model was applied in hindcasting mode, i.e. applying the model retrospectively at each time-step of the test period as if it was in real-time conditions. At each time-step, the system states are corrected using the new observations and the data assimilation scheme, and the model produces forecasts with the corrected states as initial conditions and scenarios of future rainfall as inputs. In an operational context, such scenarios are produced by weather forecast centres (e.g., MétéoFrance or the European Centre for Medium-range Weather Forecast, ECMWF). The quality of rainfall forecasts impacts the performances of flood forecasting models (see e.g., Cloke and Pappenberger 2009; Rabuffetti and Barbero 2005), but archives of past precipitation forecasts were not available and this question is out of the scope of this study. Here two simple forecasting scenarios were considered:

- Scenario P0 : zero future rainfall. This assumption represents an unfavourable sce-

377 nario in the context of flood forecasting but is the default option when no rainfall
378 forecast is available.

- 379 • Scenario PP : *perfect* rainfall forecast corresponding to the *a posteriori* observations,
380 i.e. the best available precipitation estimates.

381 Using the rainfall observed *a posteriori* as future scenario (PP) put the model in an ideal
382 situation, i.e. with limited rainfall uncertainty, and gives very optimistic results on model
383 performances compared to what it could be in real time. The P0 scenario is investigated to
384 test the model in more difficult conditions, i.e. without any information on future rainfall,
385 which is very pessimistic in the perspective of flood forecasting.

386 Evaluation criteria

387 As mentioned in the introduction section, three days of anticipation are requested in
388 Paris to organize evacuation and rescue. The maximum lead time considered in this study
389 was then 72 hours. Model performance analysis was evaluated using the RMSE between
390 discharge observations and forecasts for different lead times L ranging from 1 to 72 hours:

$$391 \text{RMSE}(L) = \sqrt{\frac{1}{N_{\mathcal{F}}} \sum_{k+L \in \mathcal{F}} (Q_{obs}(k+L) - Q_{for}(k+L))^2} \quad (14)$$

392 where $Q_{obs}(k+L)$ and $Q_{for}(k+L)$ are the observed and forecast downstream discharges at
393 time $k+L$, respectively, \mathcal{F} a set of time-steps of the test period when the model is evaluated
394 and $N_{\mathcal{F}}$ the number of time-steps in \mathcal{F} . The computation was restricted to high-flow periods,
395 here defined above a flood threshold equal to the 0.95 (non-exceedance) quantile Q_{95} of the
396 flow duration curve:

$$397 \mathcal{F} = \{k | Q_{obs}(k) \geq Q_{95}\} \quad (15)$$

398 This flood threshold was chosen to uniformly treat all the stations. As a benchmark,
399 we also computed the RMSE for the persistence model which assumes that forecast flows
400 equal the observed flow at the time of issuing the forecast, i.e. flows remain unchanged in

401 the future. Note that other evaluation scores and criteria could have been considered, some
 402 measuring the modelling error at each time step and others measuring the capacity of the
 403 model to forecast the exceedance of a threshold. RMSE was chosen here because it integrates
 404 all the model errors over the time series, and put more weight (due to the square) to large
 405 errors that generally occur in high flow conditions. Also this is a very common criterion,
 406 which appears in widely used efficiency measures (like the Nash-Sutcliffe criterion or the
 407 persistence index).

408 To compare the performance of the various tested configurations, we introduced another
 409 criterion called Forecast Performance Index (FPI), that accounts for the improvement for
 410 leading horizons ranging from 1 to 72 h, compared to the persistence model:

$$411 \quad \text{FPI} = \frac{1}{72} \sum_{L=1}^{72} \frac{1}{2} \left(\frac{\text{RMSE}^{PP}(L)}{\text{RMSE}^{PERS}(L)} + \frac{\text{RMSE}^{P0}(L)}{\text{RMSE}^{PERS}(L)} \right) \quad (16)$$

412 where RMSE^{PP} and RMSE^{P0} are the RMSE criteria for the PP and P0 scenarios for a given
 413 configuration, while RMSE^{PERS} corresponds to the persistence model. FPI is lower than 1
 414 for a configuration that has better performances than the persistence model. Note that FPI
 415 only gives an overview of the overall performances, since it does not inform on performance
 416 differences between small and large lead times or between P0 and PP scenarios.

417 The objective function used for parameter calibration is the RMSE computed in simu-
 418 lation mode. To give an overview of model performance in simulation mode, an evaluation
 419 of model performance was also made in calibration and validation using the Nash-Sutcliffe
 420 efficiency (NSE, Nash and Sutcliffe 1970).

421 **Tested configurations**

422 The main objective was to evaluate model sensitivity at the outlet (Paris-Austerlitz sta-
 423 tion) using various upstream configurations. The simplest configuration is to apply the
 424 model in a lumped mode, i.e. only considering the Paris-Austerlitz station. This configura-
 425 tion serves as a reference and is noted A0 in the following.

426 The performance analysis was done in two steps. First, only one station upstream of
427 Paris-Austerlitz among the four closest stations (Bazoches-lès-Bray, Courlon-sur-Yonne, Lo-
428 ing at Episy, La Ferté-sous-Jouarre) is considered. The four corresponding configurations
429 are noted A1 to A4 respectively. Two additional configurations were considered by including
430 the four upstream stations within the Yonne basin (Dornecy, Arcy-sur-Cure, Dissangis and
431 Aisy-sur-Armanon, noted A2') or the second upstream station on the Marne basin (Châlon-
432 sur-Marne, noted A4'). This aimed at evaluating the usefulness of these upstream stations.
433 It can be expected that discharge forecasts be improved at the Courlon-sur-Yonne station in
434 the case of A2' and at the Ferté-sous-Jouarre station in the case of A4'. A summary of the
435 six A configurations is given in Table 2.

436 The four configurations with a single upstream station were ranked by increasing perfor-
437 mance for flow forecasting at Paris-Austerlitz station using the RMSE(L) criterion. Then we
438 tested several configurations with an increasing number of upstream stations, first including
439 the station that provided the most successful results among the A1-A4 configurations, then
440 the second most successful station, etc. These configurations will be noted B1 to B4.

441 **RESULTS AND DISCUSSION**

442 **Results with only one upstream station**

443 *Calibration/validation results in simulation mode*

444 For each configuration A1 to A4, models were first evaluated in simulation mode by
445 applying the split-sample test previously described. Fig. 7 shows the NSE values at Paris-
446 Austerlitz station obtained in simulation mode for periods P1 and P2 and for both calibration
447 and validation steps. First, all the NSE values are larger than 0.70 which is a quite good score
448 (see e.g., Chiew and McMahon 1993). Second, adding one upstream station in the model
449 always improved the NSE at Paris-Austerlitz station, except for the A1 configuration (i.e.
450 considering the Marne basin) on the P1 period (for identification as well as for the validation)
451 which is due to the fact that no data are available before 1999 at Bazoches-lès-Bray (station

452 considered in A1). Moreover, for each period, NSE values are very close for identification
453 and validation, which is an indication of the consistency of the optimised parameter sets.

454 In spite of good NSE values for the different configurations, assimilating discharge data
455 proves of high added value. Indeed, whatever the configuration, the NSE is very close to
456 1 when the Kalman filter is applied. This shows that assimilating discharge data allows to
457 efficiently correct the model state that is then used as the initial state in the forecast step.

458 *Comparison of results in forecasting mode*

459 Forecast performances of each configuration A1 to A4 (including A2' and A4') are com-
460 pared to those of A0 for both scenarios PP (perfect rainfall foreknowledge) and P0 (zero
461 future rainfall). Figure 8 shows the evolution of RMSE(L) averaged over P1 and P2 periods
462 in validation mode. The performance of the persistence model is also plotted.

463 First it can be mentioned that performance curves are almost similar between the PP
464 and P0 scenarios up to a certain lead time (between ten and 20 hours in most cases). This
465 corresponds to the time response of the catchment: before this limit, the catchment response
466 only depends on the rainfall fallen before the time of issuing the forecast and is therefore
467 insensitive to future rainfall hypothesis. Second, as expected, the performance with the
468 P0 scenario is always worse than with the PP scenario and the longer the lead time, the
469 larger the difference. Model performance with P0 scenario becomes even worse than for the
470 persistence model for lead times longer than 50 hours, whatever the configuration.

471 The comparison between A0 and A1 (first line in Figure 8) shows that including the
472 Bazoches-lès-Bray station (Seine) does not improve the performance of the downstream
473 discharge forecast. As stated before, this is explained by the fact that no data are available
474 at this station before 1999. Indeed, on the 1994-1998 period, the discharge estimated at this
475 station is not corrected during the assimilation process, which impacts the results.

476 The A2 configuration (second line), in which the gauging station at the outlet of the
477 Yonne basin is considered, presents significantly better results than A0. This means that
478 the Yonne tributary provides a significant part of the variability of the Seine streamflow

479 and that the TGR model with the Kalman Filter is able to well reproduce the discharge
480 at the outlet of the Yonne basin. Including the four stations within the Yonne basin (i.e.
481 A2' configuration) leads to an notable improved forecast at Courlon-sur-Yonne (Figure 9)
482 that results in a better prediction for Paris-Austerlitz (3rd line, Figure 8), namely for the
483 P0 scenario.

484 The A0-A3 comparison (fourth line) shows a very small improvement for the P0 scenario
485 and for large lead times when the downstream station of the Loing basin is taken into account.
486 This is explained by the fact that this basin only makes a limited contribution to floods on
487 the downstream part of the Seine (the Loing represents only 9 % of the Seine basin area).

488 Finally, forecast performances of A0 and A4 configurations (fifth line) are quite similar.
489 This result seems surprising since the Marne basin is a quite large contributor to the down-
490 stream flow. The difficulty for the hydrological model to satisfactorily simulate the behaviour
491 of this basin may partly explain this result. The integration of the Châlons-sur-Marne sta-
492 tion (configuration A4') yielded substantially better results at the Ferté-sous-Jouarre (see
493 Figure 10), hence indicating the benefit of upstream observations. However benefits at
494 Paris-Austerlitz remained modest (last line in Figure 8). The quality of data at the Ferté-
495 sous-Jouarre station is also potentially responsible for limited performances. Indeed poor
496 data quality could lead to corrected system states far from the reality. This assumption is
497 explored in the next section.

498 As expected, the lowest FPI value is obtained with configuration A2, which has the high-
499 est upstream catchment area and mean discharge (Table 1). On the other hand, configuration
500 A3 which obtained the second performance results, has the lowest upstream catchment area
501 and mean discharge. This shows that best performances are not necessarily obtained when
502 considering the most contributing upstream basins, in terms of both catchment area and
503 mean discharge.

504 **Results with several upstream stations**

505 *Configurations*

506 In this section, the successive inclusion of several upstream stations is considered. Given
507 the previous results, the upstream stations were sorted by decreasing gain in forecast ef-
508 ficiency (FPI) and the following order was chosen to successively include stations in the
509 semi-distributed model: (1) Courlon-sur-Yonne, (2) Episy, (3) Bazoches-lès-Bray and (4) La
510 Ferté-sous-Jouarre. These four new configurations will be named B1 to B4 hereafter and
511 will also be compared to the reference configuration, noted B0, representing the entire basin
512 without upstream stations. Note that configurations B0 and B1 are identical to A0 and A2,
513 respectively.

514 *Calibration/validation results in simulation mode*

515 As for configurations A, Fig. 11 shows the NSE efficiency at Paris-Austerlitz station
516 for configurations B. For period P2, the NSE always increase when new stations are added,
517 leading to very high values (up to 0.95). The only exception is for the validation step for
518 configuration B4. This case is discussed in the next section. Concerning period P1, there is a
519 loss of efficiency from B1 to B2, which is probably due to the lack of data at Bazoches-lès-Bray
520 before 1999. Besides, the parameter values seem to be still consistent since identification
521 and validation NSE values remain close for each period.

522 *Comparison of results in forecasting mode*

523 Each configuration (including n upstream stations) was compared with the previous one
524 (including $n-1$ stations) through the RMSE(L) and FPI criteria to visualize the improve-
525 ments due to the successive addition of gauging station flows for use in data assimilation.
526 Results are presented in Figure 12.

527 The B0-B1 comparison (first line) is identical to the A0-A2 comparison, showing the
528 results of including the station Courlon-sur-Yonne. The integration of the Loing basin only
529 marginally improves performance (second line). The B2-B3 comparison (third line) also
530 shows that the integration of the upstream station on the Seine only slightly improves per-

531 formances. Remember that for this station, the performance is further enhanced when one
532 considers only the period after 1999 without any gap. Finally, as shown by comparing B3-B4
533 (fourth line), the inclusion of the station at La Ferté-sous-Jouarre (Marne) deteriorates the
534 forecast performance, even when the station of Châlons-sur-Marne is integrated (configura-
535 tion B4'). This result is quite surprising as one might expect *a priori* that the integration
536 of additional data in the data assimilation algorithm should lead to a better simulation of
537 the downstream discharge.

538 As stated previously, a possible cause of this degradation is the quality of data at La
539 Ferté-sous-Jouarre station. Unfortunately, no information on the data quality is available
540 that could support this assumption. As a workaround, we increased the value related to
541 the observations at this station in the measurement noise covariance matrix (R), which
542 is equivalent to considering that measurements from this station are more uncertain. By
543 doing this, the Kalman Filter gives less weight to this observation in the update step. The
544 resulting configuration is called B4R. Figure 13 compares the performances for configuration
545 B4 and B4R. Increasing the measurement noise correlation of this station highly increased
546 the forecast performances. The value of FPI decreased from 0.988 to 0.754. This result
547 clearly supports the assumption of poor data quality. It also shows how information about
548 data quality, when available, can be taken into account in the data assimilation procedure.

549 Finally, Figure 14 shows the FPI values for all the tested configurations and for the GRP
550 model. These results show that configuration B3 provides the best performance according
551 to the FPI criterion. The forecast performance comparison between this configuration and
552 the GRP model (currently used in operational conditions by the FFC) is presented in Figure
553 15, whereas Figure 16 shows an example of discharge forecast with GRP and B3 during
554 the major flood of 1995. The TGR semi-distributed model with configuration B3 clearly
555 outperformed the GRP lumped model (FPI of 0.722 and 0.810, respectively), namely for
556 small lead times and with the PP scenario.

557 CONCLUSION

558 The objective of this study was to investigate the sensitivity of flood forecasts to the
559 spatial distribution of inputs using a semi-distributed hydrological model (TGR). The semi-
560 distributed approach was chosen to test different degrees of spatialization. Here the spatial
561 distribution was defined by a subset of available gauging stations and related intermediate
562 basins. Forecast performances of different spatial distribution are analyzed and compared
563 to a reference lumped model (GRP) currently used operationally by the regional flood fore-
564 casting centre.

565 It is shown that the TGR model provides better forecast performance than the GRP
566 lumped model. This result was expected since, despite the linearization of the routing
567 reservoir, the TGR model uses observed upstream flow data not used by the GRP model.

568 Nevertheless, results obtained when increasing the degree of spatialization shows that
569 including more gauging stations in the model does not systematically improve its perfor-
570 mance. In an operational context, the model used has to be robust and computationally
571 efficient, and it could be of prior importance to find the optimal spatial distribution which
572 is not necessarily the one using all the available observed data. In addition, the case of
573 the Marne river shows that considering some particular stations could even deteriorate the
574 forecast performances. For such stations, we showed that increasing the measurement noise
575 covariance can highly improve the forecast performances.

576 Another important advantage of the semi-distributed approach is that it is possible to
577 handle parts of the basin with large human influences like regulated dams, especially when
578 little information on the management rules is available. Considering a station downstream
579 of the dam is a way to isolate its influence. Some current work focuses on the integration of
580 a simple reservoir module into the TGR model (Ficchi et al. 2013).

581 Finally, Lerat et al. (2012) showed that decomposing the inflows into localized and dis-
582 tributed lateral inflows improves the discharge simulation inside the basin (anywhere in the
583 main stream). Such a decomposition is possible with the routing model developed in this

584 study. Potential applications thus include the reconstruction and forecasting of the dis-
585 charge at ungauged sites and using it as input for a 2D flooding model in order to elaborate
586 prevention plans.

587 **ACKNOWLEDGMENT**

588 The authors thank Météo-France for providing the meteorological data used in this study
589 and the Seine-Moyenne-Yonne-Loing flood forecasting centre (SPC SMYL) at DRIEE Ile-de-
590 France for providing hydrological data, financial support and feedback on the results of the
591 study. Finally, we are grateful to the anonymous reviewers for their comments that helped
592 to improve the article.

593 **SUPPLEMENTAL DATA**

594 Appendixes S1-S3 are available online in the ASCE Library (www.ascelibrary.org).

595 **REFERENCES**

- 596 Amengual, A., Diomede, T., Marsigli, C., Martín, A., Morgillo, A., Romero, R., Papetti,
597 P., and Alonso, S. (2008). “A hydrometeorological model intercomparison as a tool to
598 quantify the forecast uncertainty in a medium size basin.” *Natural Hazards and Earth*
599 *System Science*, 8(4), 819–838.
- 600 Berthet, L., Andréassian, V., Perrin, C., and Javelle, P. (2009). “How crucial is it to account
601 for the Antecedent Moisture Conditions in flood forecasting? Comparison of event-based
602 and continuous approaches on 178 catchments.” *Hydrology and Earth System Sciences*
603 *Discussions*, 6(2), 1707–1736.
- 604 Billen, G., Silvestre, M., Barles, S., Mouchel, J.-M., Garnier, J., Curie, F., and Boët, P.
605 (2009). “Le bassin de la Seine. Découvrir les fonctions et les services rendus par le système
606 Seine.” *Agence de l’Eau Seine Normandie, Programme PIREN-Seine*, Fascicule, 51 p.
- 607 Brown, R. and Hwang, P. (1992). *Introduction to Random Signals and Applied Kalman*
608 *Filtering*. John Wiley and Sons.

609 Chiew, F. and Mc Mahon, T. (1993). “Assessing the adequacy of catchment streamflow yield
610 estimates.” *Australian Journal of Soil Research*, 31(5), 665.

611 Cloke, H. L. and Pappenberger, F. (2009). “Ensemble flood forecasting: A review.” *Journal
612 of Hydrology*, 375, 613–626.

613 Cole, S. J. and Moore, R. J. (2009). “Distributed hydrological modelling using weather radar
614 in gauged and ungauged basins.” *Advances in Water Resources*, 32(7), 1107–1120.

615 Duan, Q., Sorooshian, S. and Gupta, V. (1992). “Effective and efficient global optimization
616 for conceptual rainfall-runoff models..” *Water resources research*, 28(4), 1015–1031.

617 Fan, P. and Li, J. (2006). “Diffusive wave solutions for open channel flows with uniform and
618 concentrated lateral inflow.” *Advances in Water Resources*, 29(7), 1000–1019.

619 Ficchi, A., Raso, L., Jay-Allemand, M., Dorchies, D., Malaterre, P.-O., Pianosi, F., and
620 Van Overloop, P.-J. (2013). “A centralized real-time controller for the reservoir’s man-
621 agement on the Seine River using ensemble weather forecasting.” *EGU General Assembly
622 Conference Abstracts*, 15, 10420.

623 Kalman, R. (1960). “A New Approach to Linear Filtering and Prediction Problems.” *Journal
624 of Basic Engineering*, 82-D, 35–45.

625 Kealey, T. (2007). “Rising levels of discontent.” *The Times*, August 20, Science NoteBook.

626 Klemes, V. (1986). “Operational testing of hydrological simulation models.” *Hydrological
627 Sciences Journal*, 31(1), 13–24.

628 Lacaze, Y., Chesneau, S., Raimbault, E., Piotte, O., Silva, J.-P., Perrin, C., Andreas-
629 sian, V., Berthet, L., Coron, L., and Fortier-Filion, T.-C. (2011). “Les modèles de
630 prévision opérationnels d’aujourd’hui auraient-ils été fiables sur la crue de 1910 ? Analyse
631 rétrospective critique sur une base de données de 1910 (Would the currently operational
632 models have been reliable to forecast the 1910 flood event? Critical analysis using a
633 historical database).” *La Houille Blanche*, (1), 22–29.

634 Lerat, J., Perrin, C., Andréassian, V., Loumagne, C., and Ribstein, P. (2012). “Towards ro-
635 bust methods to couple lumped rainfall-runoff models and hydraulic models: A sensitivity

636 analysis on the Illinois River.” *Journal of Hydrology*, 418-419, 123–135.

637 Liu, Y., Weerts, A. H., Clark, M., Franssen, H. J. H., Kumar, S., Moradkhani, H., Seo,
638 D. J., Schwanenberg, D., Smith, P., van Dijk, A. I. J. M., van Velzen, N., He, M., Lee,
639 H., Noh, S. J., Rakovec, O., and Restrepo, P. (2012). “Advancing data assimilation in
640 operational hydrologic forecasting: progresses, challenges, and emerging opportunities.”
641 *Hydrology and Earth System Sciences*, 16(10), 3863–3887.

642 McMillan, H. K., Hreinsson, E. O., Clark, M. P., Singh, S. K., Zammit, C., and Uddstrom,
643 M. J. (2013). “Operational hydrological data assimilation with the recursive ensemble
644 Kalman filter.” *Hydrology and Earth System Sciences*, 17(1), 21–38.

645 Mendoza, P. A., McPhee, J., and Vargas, X. (2012). “Uncertainty in flood forecasting: A
646 distributed modeling approach in a sparse data catchment.” *Water Resources Research*,
647 48(9), W09532.

648 Munier, S. (2009). “Modélisation intégrée des écoulements pour la gestion en temps réel
649 d’un bassin versant anthropisé (Integrated flow modeling for real time management of an
650 anthropized basin).” Ph.D. thesis, AgroParisTech, Montpellier,

651 Munier, S., Litrico, X., Belaud, G., and Malaterre, P.-O. (2008). “Distributed approxima-
652 tion of open-channel flow routing accounting for backwater effects.” *Advances in Water
653 Resources*, 31(12), 1590–1602.

654 Nash, J. and Sutcliffe, J. (1970). “River flow forecasting through conceptual models part I ?
655 A discussion of principles.” *Journal of Hydrology*, 10(3), 282–290.

656 Nester, T., Kirnbauer, R., Parajka, J., and Blöschl, G. (2012). “Evaluating the snow com-
657 ponent of a flood forecasting model.” *Hydrology Research*, 43(6), 762.

658 Oudin, L., Hervieu, F., Michel, C., Perrin, C., Andréassian, V., Anctil, F., and Loumagne, C.
659 (2005). “Which potential evapotranspiration input for a lumped rainfall?runoff model?”
660 *Journal of Hydrology*, 303(1), 290–306.

661 Perumal, M., Sahoo, B., Moramarco, T., and Barbetta, S. (2009). “Multilinear Muskingum
662 Method for Stage-Hydrograph Routing in Compound Channels.” *Journal of Hydrologic*

663 *Engineering*, 14(7), 663–670.

664 Rabuffetti, D. and Barbero, S. (2005). “Operational hydro-meteorological warning and real-

665 time flood forecasting: the Piemonte Region case study.” *Hydrol. Earth Syst. Sci.*, 9,

666 457–466.

667 Refsgaard, J. C. (1997). “Validation and intercomparison of different updating procedures

668 for real-time forecasting.” *Nordic Hydrology*, 28(2), 65–84.

669 Smith, M. B., Koren, V., Zhang, Z., Zhang, Y., Reed, S. M., Cui, Z., Moreda, F., Cosgrove,

670 B. A., Mizukami, N., and Anderson, E. A. (2012). “Results of the DMIP 2 Oklahoma

671 experiments.” *Journal of Hydrology*, 418-419, 17–48.

672 Todini, E. (2007). “Hydrological catchment modelling: past, present and future.” *Hydrology*

673 *and Earth System Sciences*, 11(1), 468–482.

674 Vidal, J.-P., Martin, E., Franchistéguy, L., Baillon, M., and Soubeyroux, J.-M. (2010).

675 “A 50-year high-resolution atmospheric reanalysis over France with the Safran system.”

676 *International Journal of Climatology*, 30(11), 1627–1644.

677 Viennot, P., Ducharne, A., Habets, F., Lamy, F., and Ledoux, E. (2009). “Hydrogéologie

678 du bassin de la Seine.” *Agence de l’Eau Seine-Normandie, Programme PIREN-Seine*,

679 Fascicule, 55 p.

680 Villion, G. (1997). “Rôle des lacs-réservoirs amont : les grands lacs de Seine.” *La Houille*

681 *Blanche*, 8, 51–56.

682 Welles, E., Sorooshian, S., Carter, G., and Olsen, B. (2007). “Hydrologic verification. A call

683 for action and collaboration.” *Bull. Amer. Meteor. Soc.*, 88 (4), 503–511.

684 Young, P. C. (1974). “Recursive approaches to time series analysis.” *Bull. Inst. Math. Appl.*,

685 10, 209–224.

686 Young, P. C. (2002). “Advances in real-time flood forecasting..” *Philosophical transactions.*

687 *Series A, Mathematical, physical, and engineering sciences*, 360(1796), 1433–50.

688 **List of Tables**

689 1 List of the flow gauging stations. The mean discharge and the percentage of
690 missing values are given for the 1995-2009 period. 29
691 2 List of tested configurations A0 to A4, and gauging stations considered. . . . 30

TABLE 1. List of the flow gauging stations. The mean discharge and the percentage of missing values are given for the 1995-2009 period.

Station code	Station name	River	Area (km ²)	Mean discharge (m ³ /s)	Missing values (%)
H1940020	Bazoches-lès-Bray	Seine	10100	85.2	35.6
H2051010	Dornecy	Yonne	754	10.0	7.8
H2182010	Arcy-sur-Cure	Cure	1182	16.4	9.6
H2332020	Dissangis	Serein	636	4.5	6.1
H2452020	Aisy-sur-Armanon	Armanon	1350	13.1	7.5
H2721010	Courlon-sur-Yonne	Yonne	10700	99.8	7.3
H3621010	Episy	Loing	3900	20.5	7.4
H5201010	Châlon-sur-Marne	Marne	6280	75.7	7.0
H5321010	La Ferté-sous-Jouarre	Marne	8818	97.9	12.8
H5920010	Paris-Austerlitz	Seine	43800	343.7	11.1

TABLE 2. List of tested configurations A0 to A4, and gauging stations considered.

Configuration	Station names
A0	Paris-Austerlitz
A1	Paris-Austerlitz, Bazoches-lès-Bray
A2	Paris-Austerlitz, Courlon-sur-Yonne
A2'	Paris-Austerlitz, Courlon-sur-Yonne, Dornecy, Arcy-sur-Cure, Dissangis and Aisy-sur-Armanon
A3	Paris-Austerlitz, Episy
A4	Paris-Austerlitz, La Ferté-sous-Jouarre
A4'	Paris-Austerlitz, La Ferté-sous-Jouarre, Châlon-sur-Marne

692 **List of Figures**

693 1 The Seine River basin at Paris (43,800 km²), and the networks of raingauges
694 and flow gauging stations used in the study. The station details corresponding
695 to the codes shown on the map are given in Table 1. 33

696 2 Schematic representation of the hydrology-routing coupled model (PE and P
697 are the potential evapotranspiration and rainfall inputs to the model, Q stands
698 for streamflow). The drained area curve is used for the spatial discretization
699 inside the intermediate basin. 34

700 3 (a) Example of hydrological discretization based on the gauging station net-
701 work and (b) corresponding modelling scheme. 35

702 4 Structure of the hydrological model. 36

703 5 Flow routing model scheme. 37

704 6 The TGR coupled model scheme for one intermediate basin. 38

705 7 Nash-Sutcliffe efficiency obtained at Paris-Austerlitz station in simulation
706 mode for A0 to A4 configuration in identification and validation for the two
707 test periods P1 and P2. 39

708 8 Forecast performance obtained in validation by the TGR model and the persis-
709 tence model (PERS) at the Paris-Austerlitz station for the six configurations
710 (see Table 2) using PP and P0 rainfall scenarios. Lead times range from 1 to
711 72 hours. Two configurations are compared in each case, illustrated on the
712 left and right hand sides of the graph. 40

713 9 Forecast performance obtained in validation by the TGR model and the per-
714 sistence model (PERS) at the Courlon-sur-Yonne station for the A2 and A2'
715 configurations using PP and P0 rainfall scenarios. Lead times range from 1
716 to 72 hours. 41

717	10	Forecast performance obtained in validation by the TGR model and the persistence model (PERS) at the La Ferté-sous-Jouarre station for the A4 and	
718		A4' configurations using PP and P0 rainfall scenarios. Lead times range from	
719		1 to 72 hours.	42
720			
721	11	Nash-Sutcliffe efficiency obtained at Paris-Austerlitz station in simulation	
722		mode for B0 to B4 configuration in identification and validation for the two	
723		test periods P1 and P2.	43
724	12	Forecast performance obtained in validation by the TGR model and the persistence model (PERS) at the Paris-Austerlitz station for the B configurations	
725		using PP and P0 rainfall scenarios. Lead times range from 1 to 72 hours. Two	
726		configurations are compared in each case, illustrated on the left and right hand	
727		sides of the graph.	44
728			
729	13	Forecast performance obtained in validation by the TGR model with configurations B4 and B4R, and the persistence model (PERS) at the Paris-Austerlitz	
730		station using PP and P0 rainfall scenarios. Lead times range from 1 to 72	
731		hours.	45
732			
733	14	Forecast Performance Index for all the tested configurations and for the GRP	
734		model.	46
735	15	Forecast performance obtained in validation by the TGR model (configuration B3), the GRP model and the persistence model (PERS) at the Paris-Austerlitz	
736		station using PP and P0 rainfall scenarios. Lead times range from 1 to 72	
737		hours.	47
738			
739	16	Example of discharge forecast by the TGR model (configuration B3) and the GRP operational model during the 1995 main flood event with a 72-hour lead	
740		time and for PP and P0 scenarios.	48
741			

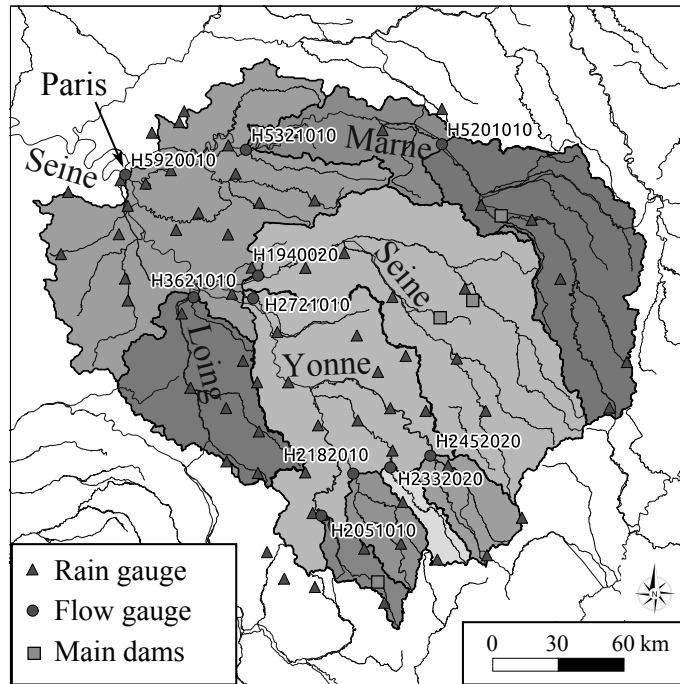


FIG. 1. The Seine River basin at Paris (43,800 km²), and the networks of raingauges and flow gauging stations used in the study. The station details corresponding to the codes shown on the map are given in Table 1.

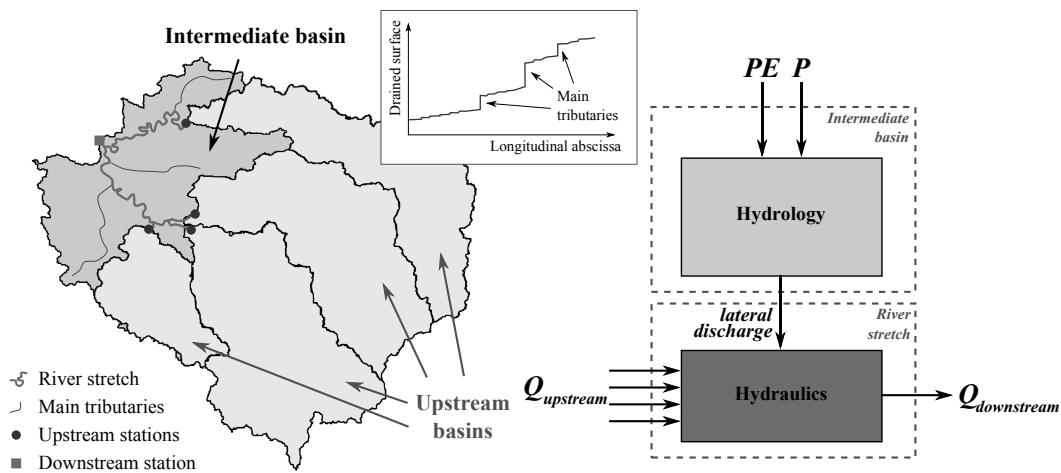


FIG. 2. Schematic representation of the hydrology-routing coupled model (PE and P are the potential evapotranspiration and rainfall inputs to the model, Q stands for streamflow). The drained area curve is used for the spatial discretization inside the intermediate basin.

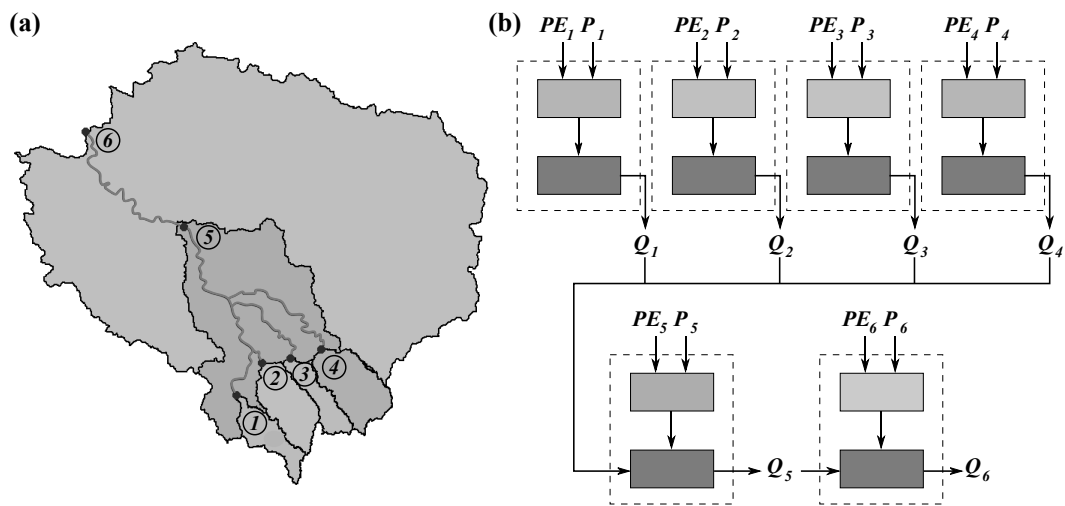


FIG. 3. (a) Example of hydrological discretization based on the gauging station network and (b) corresponding modelling scheme.

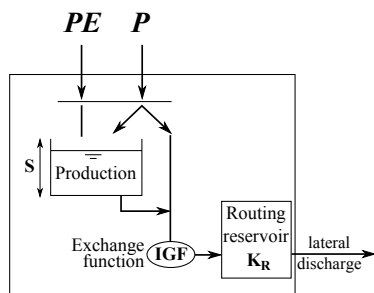


FIG. 4. Structure of the hydrological model.

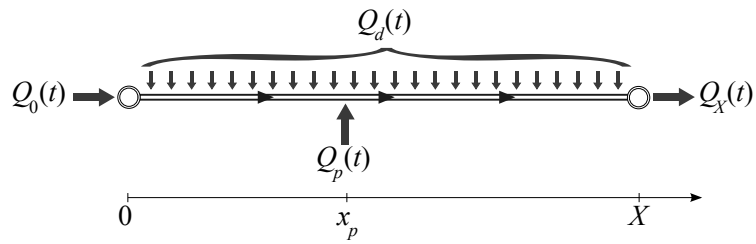


FIG. 5. Flow routing model scheme.

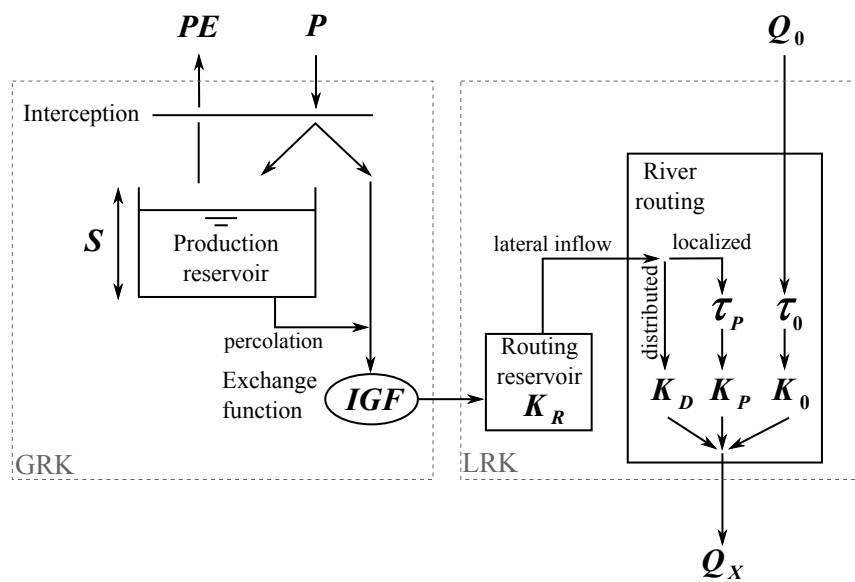


FIG. 6. The TGR coupled model scheme for one intermediate basin.

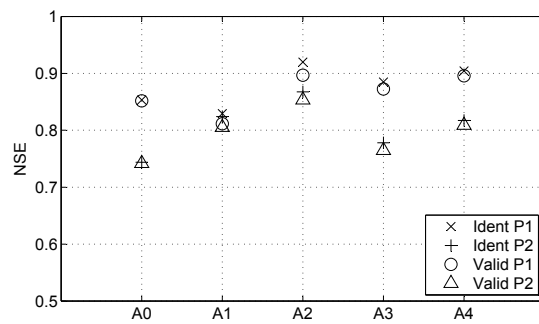


FIG. 7. Nash-Sutcliffe efficiency obtained at Paris-Austerlitz station in simulation mode for A0 to A4 configuration in identification and validation for the two test periods P1 and P2.

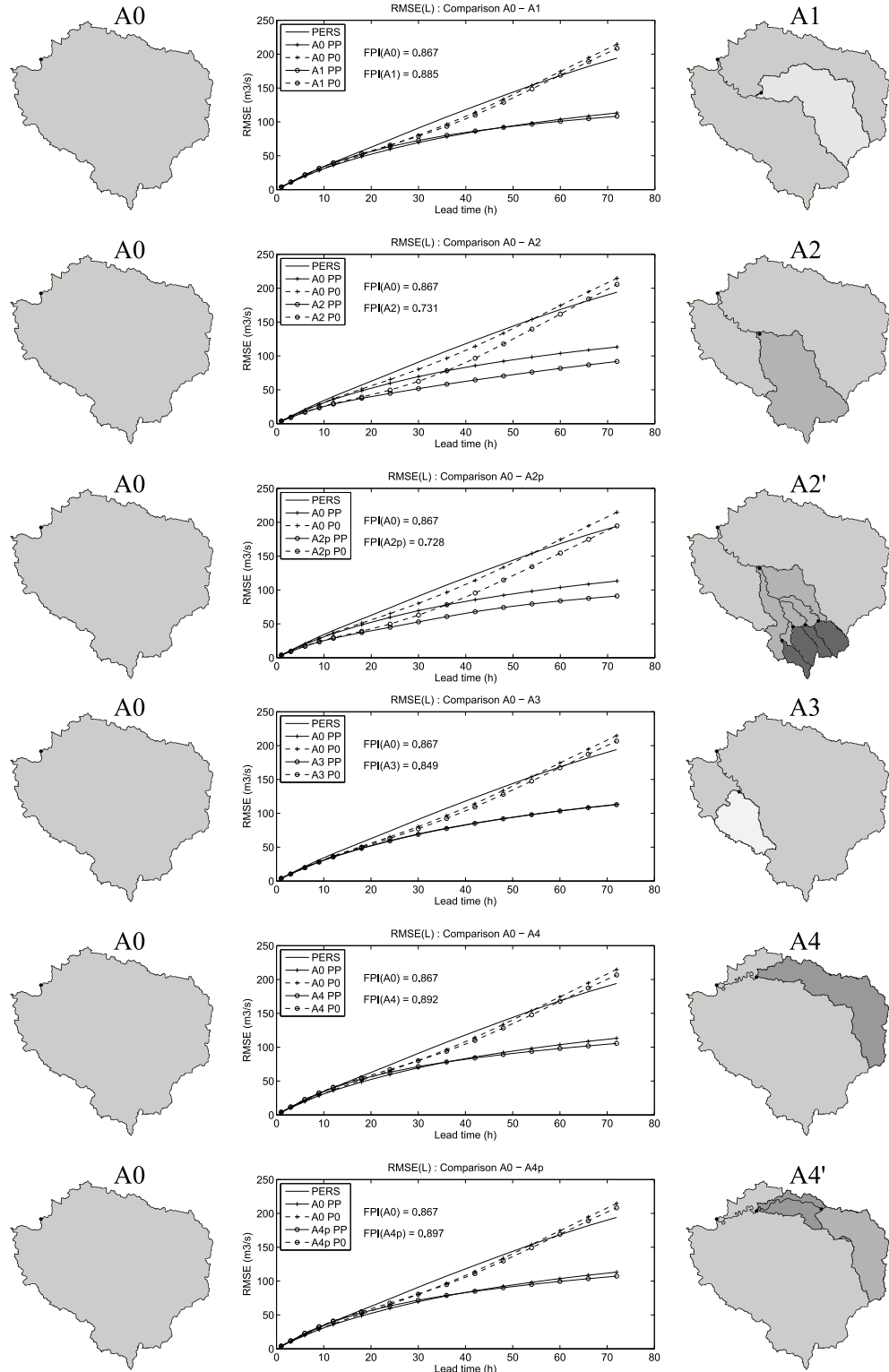


FIG. 8. Forecast performance obtained in validation by the TGR model and the persistence model (PERS) at the Paris-Austerlitz station for the six configurations (see Table 2) using PP and P0 rainfall scenarios. Lead times range from 1 to 72 hours. Two configurations are compared in each case, illustrated on the left and right hand sides of the graph.

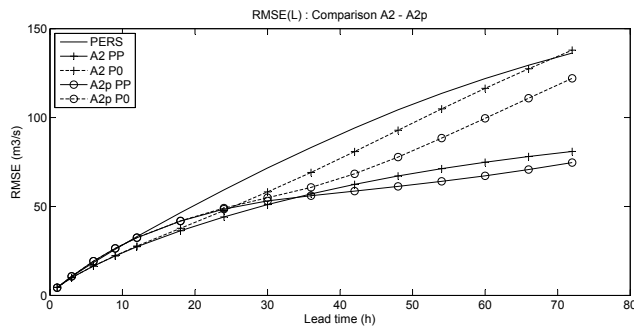


FIG. 9. Forecast performance obtained in validation by the TGR model and the persistence model (PERS) at the Courlon-sur-Yonne station for the A2 and A2' configurations using PP and P0 rainfall scenarios. Lead times range from 1 to 72 hours.

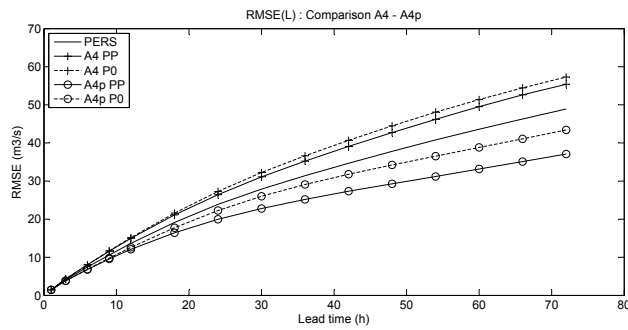


FIG. 10. Forecast performance obtained in validation by the TGR model and the persistence model (PERS) at the La Ferté-sous-Jouarre station for the A4 and A4' configurations using PP and P0 rainfall scenarios. Lead times range from 1 to 72 hours.

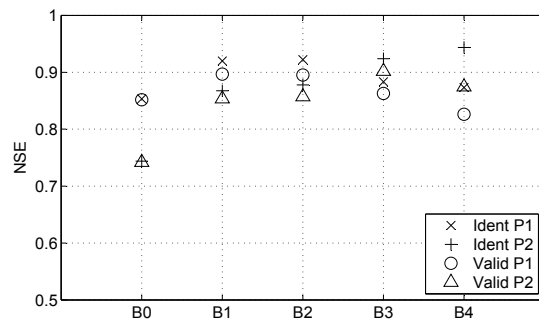


FIG. 11. Nash-Sutcliffe efficiency obtained at Paris-Austerlitz station in simulation mode for B0 to B4 configuration in identification and validation for the two test periods P1 and P2.

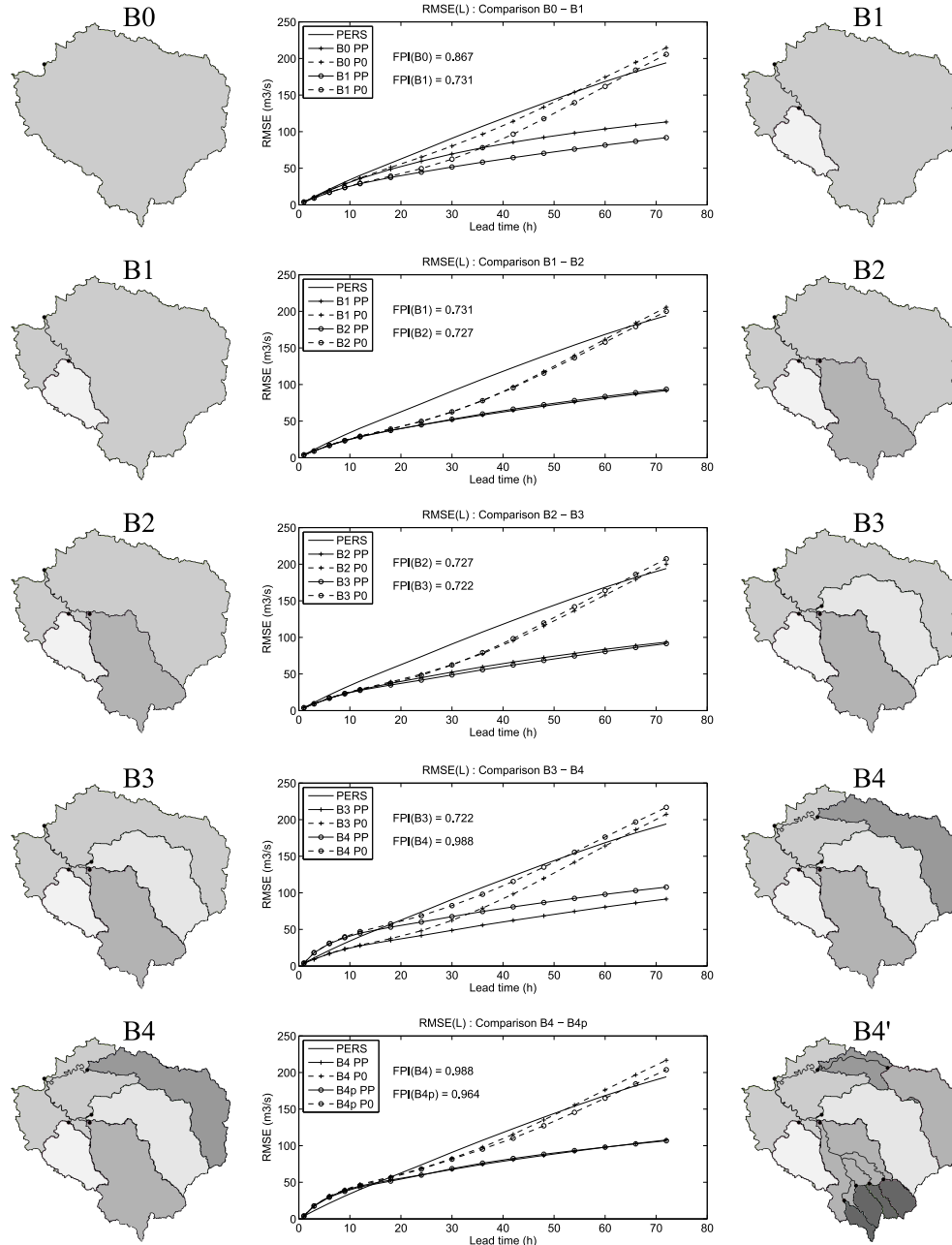


FIG. 12. Forecast performance obtained in validation by the TGR model and the persistence model (PERS) at the Paris-Austerlitz station for the B configurations using PP and P0 rainfall scenarios. Lead times range from 1 to 72 hours. Two configurations are compared in each case, illustrated on the left and right hand sides of the graph.

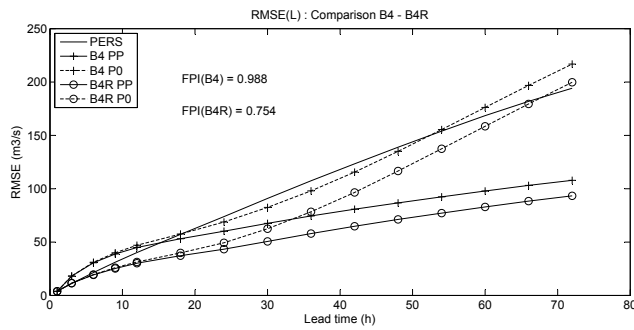


FIG. 13. Forecast performance obtained in validation by the TGR model with configurations B4 and B4R, and the persistence model (PERS) at the Paris-Austerlitz station using PP and P0 rainfall scenarios. Lead times range from 1 to 72 hours.

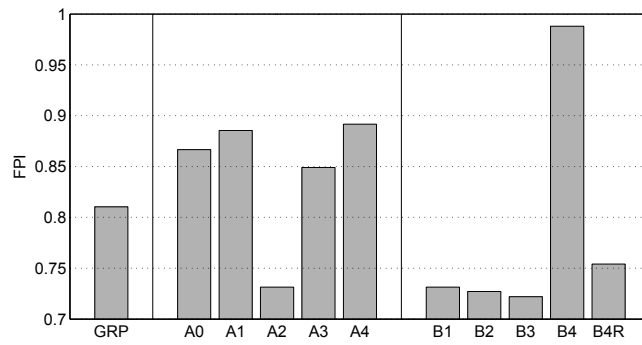


FIG. 14. Forecast Performance Index for all the tested configurations and for the GRP model.

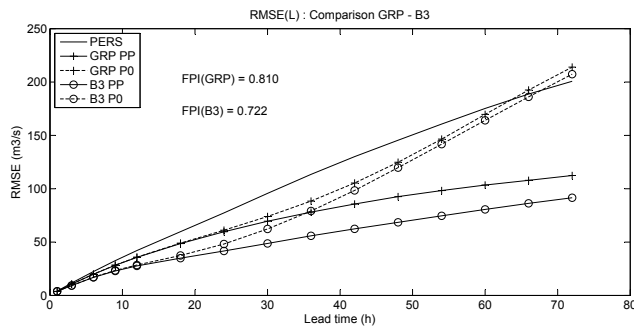


FIG. 15. Forecast performance obtained in validation by the TGR model (configuration B3), the GRP model and the persistence model (PERS) at the Paris-Austerlitz station using PP and P0 rainfall scenarios. Lead times range from 1 to 72 hours.

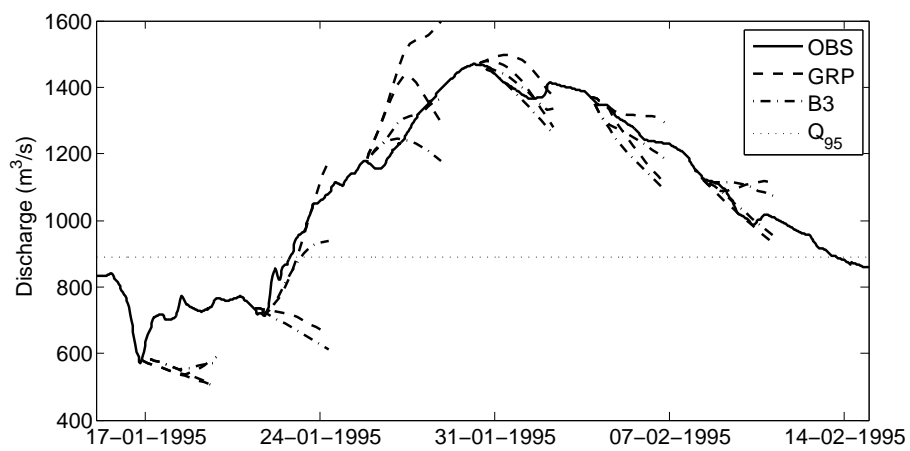


FIG. 16. Example of discharge forecast by the TGR model (configuration B3) and the GRP operational model during the 1995 main flood event with a 72-hour lead time and for PP and P0 scenarios.